Journal of Energy Storage 50 (2022) 104232

Contents lists available at ScienceDirect

Journal of Energy Storage

journal homepage: www.elsevier.com/locate/est

Research papers

Supercapacitor voltage based power sharing and energy management strategy for hybrid energy storage system

Arunkumar C.R. *, Udaya Bhasker Manthati, Srinivas Punna

Electrical Engineering Department, National Institute of Technology, Warangal, Telangana, India

ARTICLE INFO

Keywords:
DC microgrid
Supercapacitor
Energy storage system
Low pass filter
Bidirectional DC–DC converter
Battery
Power sharing

ABSTRACT

Integrating batteries accomplishes a highly reliable, efficient, and durable photovoltaic (PV) DC microgrid. Supercapacitors (SC) boost the dynamics and battery life even further, and such a combination is known as a hybrid energy storage system (HESS). The control and power splitting between the battery and SC plays a crucial role in the operation of the HESS. The most common power routing method is constant bandwidth low pass filter (LPF), the drawback of which causes slow dynamics of the control loop and significant variation in SC operating voltage leads to ringing in the DC bus voltage. Hence, this work proposes a power management scheme with a variable bandwidth filter for HESS and a power splitting control strategy to eliminate the sluggishness imposed on the battery control loop by LPF. The proposed approach has several advantages over the conventional method, including efficient SC utilization, improved battery life, and better DC bus voltage regulation. The proposed scheme is validated using simulation results. Hardware tests have been carried out to verify the proposed system's accuracy and viability.

1. Introduction

The need for newer renewable energy sources (RES) has led to the development of DC microgrid systems. The inherent DC nature of RES, energy storage systems (ESS), and loads make the DC microgrid a legitimate option for modern applications [1,2]. The ESS plays a crucial role in the development of isolated DC microgrid systems by ensuring its durability, reliability, and efficiency, characterized by its available energy (energy density), power (power density), cycle life, and response time [3]. The Ragone plot for different energy storage devices is shown in Fig. 1 to compare the maximum power capability [4]. The battery has a high energy density, allowing it to provide power for a prolonged period. However, the battery suffers from slow response time and low power density [5,6]. Hence, it is relevant to hybridize the battery with fast, responsive ESS to improve the overall performance. The advantage of hybridization is that it combines the rapid response and longer supply without altering individual ESS performances [7,8]. Well-known and emerging fast responsive ESSs (FRESS) are flywheels, superconducting magnetic energy storage (SMES), and SC [9–11]. The SC stands out among the above due to its small size and ease of use. As a result, HESS based on battery and SC is popular in PV-DC microgrid systems.

The goal of battery-SC HESS is that the battery supplies the average power demand, and SC compensates for the transient power fluctuations. In a practical scenario, three major HESS configurations integrate the battery and SC with the DC microgrid. The passive architecture directly connects the HESS to the DC microgrid [12]. The semi-active HESS architectures describe the coupling of a passive and active storage unit with the DC bus [13,14]. In [13], utilizes a bidirectional converter to link the battery to the DC bus and a passively connected SC to reduce the influence of DC bus fluctuations. Eliminating additional power converters in such topologies reduces the overall loss in the system. However, the lack of control over directly connected energy storage devices prevents effective use of its total range capacity and worsens the dynamic power sharing between the ESS. Compared to other topologies, the fully active topology gained more consideration due to the overall control and reduced size of HESS [15–21].

In typical use, the simple control strategy for HESS is the PI-LPF method [15,16]. The conventional PI control strategies are improvised by adding uncompensated battery current to SC reference current [17,18]. Further, the power splitting between battery and SC is enhanced by generating reference current based on battery current as given in [19–21]. However, the direct connected LPF in the battery control loop increases battery reference current tracking delay in all cases above. Advanced control strategies such as sliding mode control (SMC) [13,22], fuzzy logic control (FLC) [23,24], artificial neural network (ANN) [25] and model predictive control (MPC) [26,27] are found in literature. SMC provides fast dynamic performance; however,

* Corresponding author.
E-mail addresses: acr_research@student.nitw.ac.in (Arunkumar C.R.), ub@nitw.ac.in (U.B. Manthati), srinu240@student.nitw.ac.in (S. Punna).

https://doi.org/10.1016/j.est.2022.104232
Received 9 July 2021; Received in revised form 22 December 2021; Accepted 12 February 2022
Available online 4 March 2022

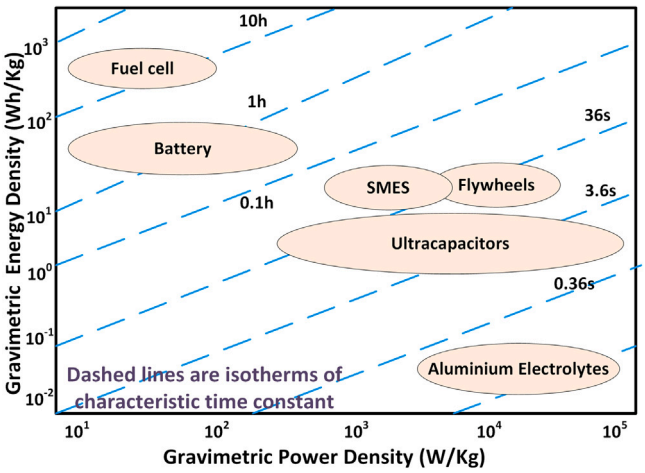

Fig. 1. Ragone plot for different energy storage systems [4].

it requires complex design procedures and is affected by chattering issues. FLC and ANN are used in HESS for energy management and voltage regulation, and they are frequently coupled with other controllers for improved performance. One significant limitation of FLC methods is that they rely on human skills and knowledge. The rule of the FLC system needs to be updated routinely. Similarly, ANN-based HESS controller performance depends on the training data used. MPC-based controllers demonstrate improved system dynamics for HESS. They do, however, need fast processors and optimization techniques for implementations.

The DC microgrid requires an energy/power management strategy (EMS/PMS) for (i) identifying the operating modes based on available PV power, (ii) to maintain the state of charge (SOC) of battery in predefined limits and SC voltage within the operating limits and (iii) to guarantee that PV, battery, and SC power is balanced in each operating modes. The traditional EMS found in the literature tries to meet the above specifications [15,28]. The EMS is further modified by splitting battery SOC range to enhance HESS operation, and dedicated SC charging schemes are introduced along with EMS can be found in [29]. Unlike the battery, the SC voltage can vary from 100% to 0% during operation. This leads to oscillations in DC bus voltage and battery current at lower SC voltages. In [30], the authors try to reduce the effect of SC voltage variation on the DC microgrid stability by proposing a novel controller design procedure. However, the optimization-based procedure complicates the approach.

From the above discussions, the issues related to HESS operation are (i) The conventional LPF control strategy slow down the system response and demands more energy at lower SC voltages, (ii) The operation of DC microgrid with lower SC voltage increases the oscillation in the system and might lead to instability. Hence this work proposes a novel control strategy that eliminates the use of LPF in battery reference current calculation. Further, an EMS is introduced to eliminate the effect of SC voltage variation on DC bus voltage. The proposed energy management scheme uses a dynamic filter for generating the SC current reference that adjusts the filter bandwidth based on SC available voltage. Also, a controlled charging scheme is added along with EMS to regulate the SC voltage conditionally. The advantage of the proposed scheme is that it reduces the DC microgrid oscillations and enables controlled charge/discharge of SC. The contributions of this work is highlighted as follows:

1 Accurate modeling based HESS controller design is presented for PV-DC microgrid. The controller parameter design procedure considers the LPF effect on HESS control loop.
2 The proposed strategy controls the battery current loop without an LPF, reducing the excessive discharge of the SC unit and delay in the battery loop.
3 The HESS control uses a variable bandwidth low pass filter (VBLPF) for power distribution in the control loop, improving SC utilization and supporting loading for prolonged periods.
4 The proposed HESS energy management strategy effectively reduces oscillations occurring at lower SC voltages.
5 A detailed comparison between the proposed VBLPF and conventional fixed-LPF based HESS controllers are analyzed in the simulation trials at different SC voltages and validated by the experimental outcome.

The rest of the paper is organized as follows. Section 2 describes a summary of proposed DC microgrid system. Section 3 presents the SC voltage based energy management strategy in detail. Section 4 discuss the control parameter design. The simulation study and experimental results are discussed in Sections 5 and 6 respectively. Finally, Section 6 summarizes the work.

2. Configuration of PV-DC microgrid

The proposed DC microgrid system integrated with HESS is shown in Fig. 2. The PV source, battery and SC are connected to the DC bus through DC-DC converters and DC loads are connected directly. The PV panel connects to the DC bus through a unidirectional DC-DC boost converter. The power converters used to connect the energy storage devices to the DC bus have bidirectional capabilities. The PV control approach employs the maximum power point tracking (MPPT) technique to get as much power out of PV panels [28]. On the other hand, the HESS control strategy aims at supporting the DC microgrid under different operating modes such as deficit power mode (DPM), surplus-power mode (SPM), and floating-power mode (FPM) [29]. In surplus/excess-power mode, the PV generation is more than the load power demand, and the ESS stores the additional PV power. In deficit-power mode, the PV generation is lower than load demand, and ESS discharges the stored power to meet the deficit. In floating mode, the PV generation matches the load demand forcing the ESS to standstill mode. The DC bus voltage regulation and load current sharing are taken care of by the HESS. The battery compensates for the steady-state power variations, while SC absorbs/delivers the transient current at the time of system disturbances. In this paper, the DC loads are represented with parallel resistances and equivalent dc loads with resistance R_L. In Fig. 2, V_{pv}, V_{sc}, V_b and V_0 are PV panel, SC, battery, and DC bus voltages respectively. The battery, PV panel and SC currents are represented by variables i_b, i_{pv} and i_{sc} respectively. L_{pv}, L_b and L_{sc} represent filter inductance of PV converter, battery converter and SCESS converter, C_0 is the filter capacitance. S_{pv}, S_{b1}, S_{b2}, S_{sc1} and S_{sc2} are control switches of power converters.

3. Proposed power splitting and EMS

This section discusses the need for a VBLPF in SC operation and designs an EMS for the smooth operation of HESS in PV-DC microgrid. The HESS EMS/PMS aims at keeping the state of charge (SOC) of the battery and SC within the operating limit. The conventional PMS considers battery SOC in the range of 80% to 20% and SC SOC in the range of 100%–20%. In contrast to the battery, SC voltage varies significantly during operation; at 50% SC voltage, only 25% of the energy is available. Also, SC SOC varies linearly with SC voltage. Hence, SC voltage variation can be considered a parameter for SC EMS monitoring instead of SC SOC. A summary of different LPF power splitting strategies is shown here.

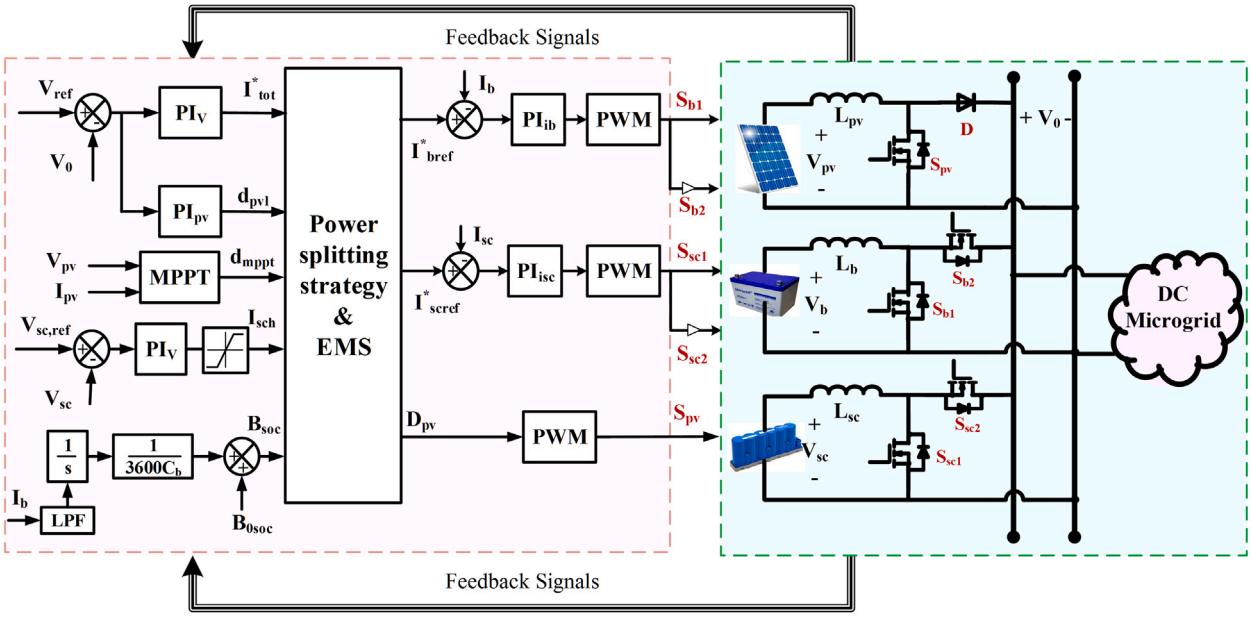

Fig. 2. The PV-DC microgrid system configuration showing HESS, PV, power electronic converters and control schemes.

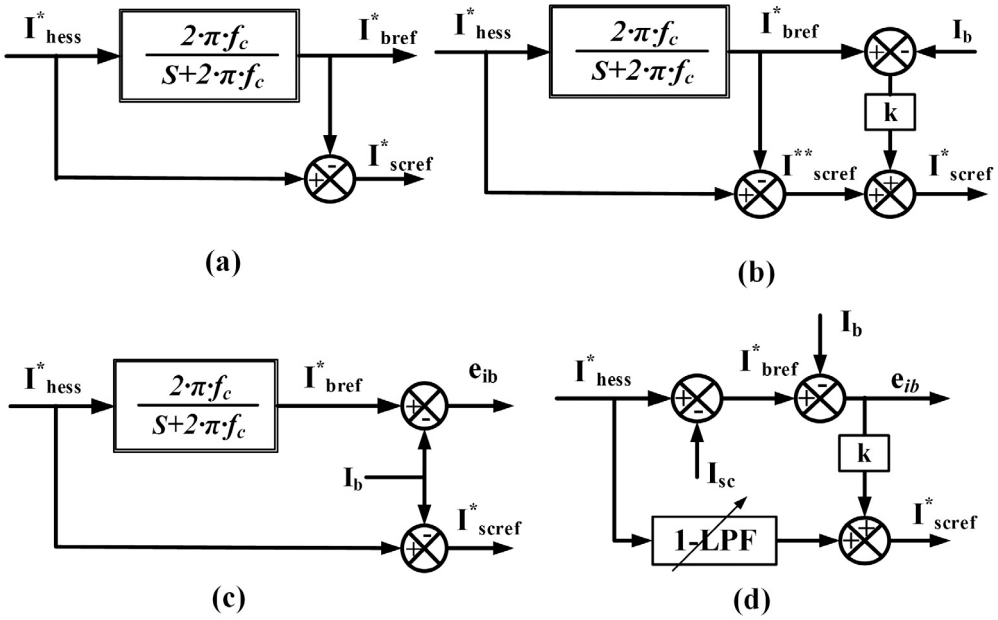

Fig. 3. The different LPF power splitting strategies (a) conventional (b) enhanced (c) modified (d) proposed.

3.1. HESS power splitting strategy

The outer voltage controller calculates the required reference current to regulate the DC bus voltage. This reference current is divided into SC current reference (i_{scref}) and battery reference current (i_{bref}) using a splitting algorithm. The LPF based power split strategy is the most common strategy for generating battery and SC current references. The total reference current is passed through an LPF to generate i_{bref} as shown Fig. 3(a) [15,16]. The SC current reference is the difference between i_{bref} and the total HESS current reference. The addition of uncompensated battery current to the i_{scref} improves the performance of the traditional power splitting strategy as illustrated in Fig. 3(b) [17, 18]. It reduces the ripple current supplied by the battery and enhances SC utilization. The LPF power splitting strategy is modified to improve the battery utilization by using the battery current to generate i_{bref} and i_{scref} as shown in Fig. 3(c) [19–21]. In all the above schemes, battery current is generated based on LPF. However, it adds delay to the battery reference current calculation. As a result, the SC discharges longer than required, and the battery current takes more time to reach the final state. Hence, an improved power splitting strategy is proposed in this work, as shown in Fig. 3(d). The HESS current reference is subtracted from the SC current to generate the current battery reference. Thus, the uncompensated battery current is added to the SC current reference to reduce the ripple.

The use of CBLPF always demands constant power from SC at the time of disturbances. As a result, even if the SC voltage is low, the HESS controller will attempt to extract the required energy from it and leads to an oscillatory response from the SC unit, as shown in Fig. 4(a). This oscillatory effect of SC voltage variation can be reduced by selecting the appropriate LPF cutoff frequency. In such cases, the bandwidth of

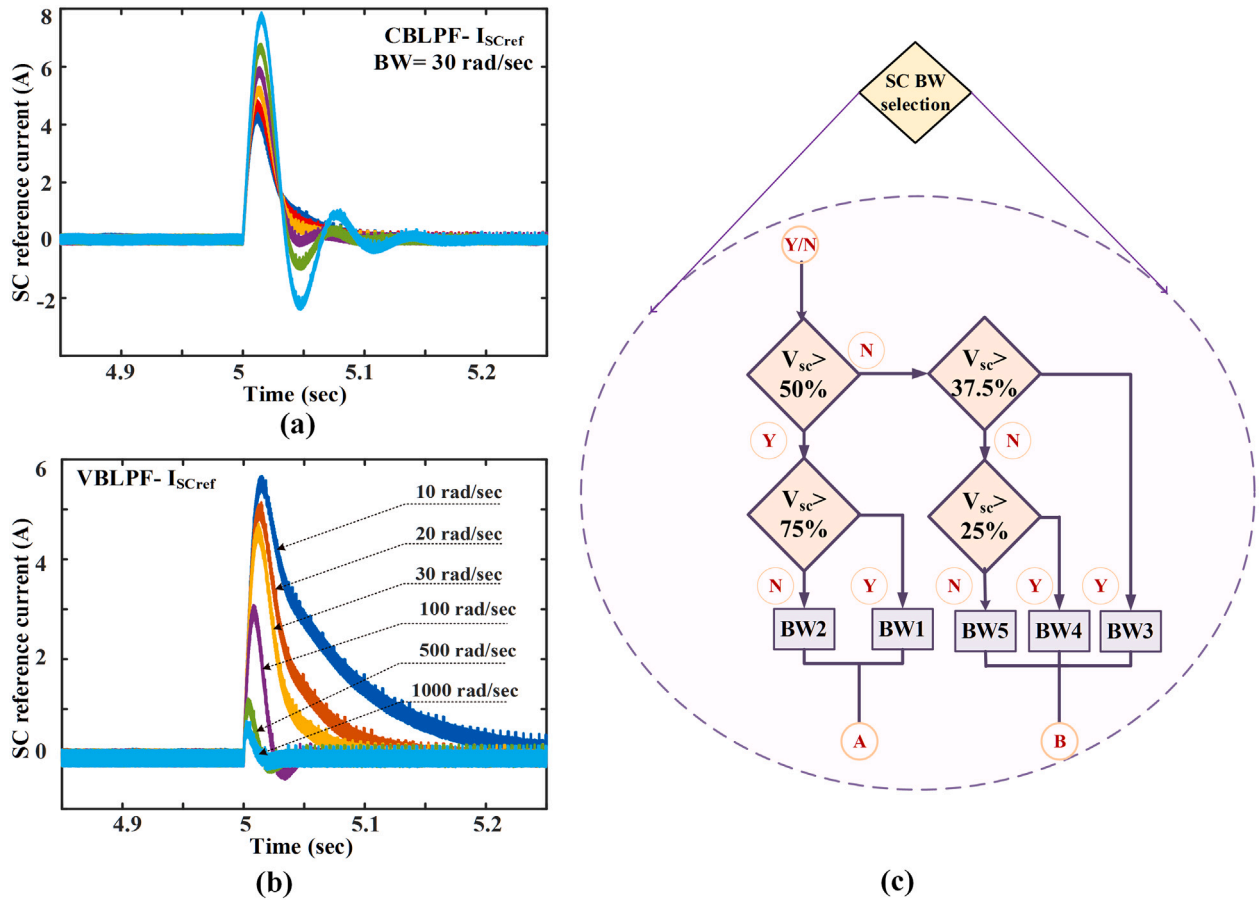

Fig. 4. SC current reference generation: (a) SC current reference generation at different SC voltage and CBLPF. (b) SC current reference generation at different SC voltage and VBLPF (c) VBLPF BW selection algorithm based on SC voltage.

the filter increases as the SC energy reduces. Consequently, it reduces the SC energy demand and the oscillations in the SC current and DC bus voltage as shown in Fig. 4(b). Further, the SC is allowed to discharge more in the range of 100%–50% SC voltage to improve the SC utilization. The VBLPF uses a Butter-worth low pass filter with unity gain and variable bandwidth in MATLAB [31]. The filter computes the required bandwidth based on the SC voltage range.

3.2. Energy management strategy

The importance of SC-EMS is to ensure proper power balance of DC microgrid under all conditions. In the proposed EMS, VBLPF based energy management for SC proposes along with the battery state of charge (B_{SOC}) management. The EMS decides the operating mode based on the I^*_{bref}. The EMS is formed to meet the following operational goals; (i) to assess and decide the operating mode of DC microgrid system based on I^*_{bref}, (ii) to maintain battery SOC B_{SOC} and SC voltage within the operating limits (iii) Allocate charging of SC based on B_{SOC} such that eliminate the current oscillation at lower SOC (iv) to make the battery to respond at the time of steady-state and SC at the time transient state only, and (v) to ensure the power balance between PV, battery and SC at each operating mode. Also, the suggested EMS does not require weather forecasts or load current/power measurements for determining the modes of operation.

The main operating modes in a PV-DC microgrid system are SPM and DPM. The FPM is added with DPM to simplify the operation. Each main mode is divided into four sub-modes based on the available battery SOC as shown in Fig. 5. They are (Mode-I) 50% < B_{soc} < 80% (Mode-II) 20% < B_{soc} < 50% (Mode-III) B_{soc} < 20% (Mode-IV) B_{soc} > 80%. In each sub-mode, V_{sc} is monitored and bandwidth selects for operation. The 75% of stored energy in an SC is available at 50% of the voltage range. So the VBLPF BW is selected to increase the utilization of SC at high voltage ranges. When the voltage is between 75% to 100%, the LPF BW is BW1= 10 rad/sec, such that SC can supply more current for a longer duration. If the voltage is between 50% to 75%, the BW changes to BW2 = 20 rad/sec. When the SC voltage reaches 50% to 37.5%, the LPF BW changes to BW3 = 30 rad/sec. The BW is BW4= 100 rad/sec when the SC voltage is between 37.5% and 25%. The BW is BW5= 500 rad/sec for below 25% SC voltage. Further, the EMS allows the SC to charge from the DC bus based on energy availability. The algorithm for selecting VBLPF bandwidth based on SC voltage is pictured in Fig. 4(c). A detailed EMS for HESS is shown in Fig: 5. The following summarizes the operation of the proposed EMS.

*(1) Deficit power mode, (I_{bref} *> 0)*: In DPM, the PV generation is less than load demand. Hence, the average current (I_{bref} *> 0) is greater than or equal to zero. There are four sub-modes to describe the DPM explained as following.

Mode-I 50% < B_{soc} < 80% : In this mode, PV power is insufficient to supply load demand. The battery operates in discharging mode. SC operates with lower BW ranges if the available voltage is more than 37.5%. SC is allowed to charge in this mode due to battery power availability as shown in Fig. 5.

Mode-II 20% < B_{soc} < 50% : In this mode, battery power is limited to supply only the load demand. Therefore SC is restricted from charging as shown in Fig. 5.

Mode-III B_{soc} < 20% : The battery and SC cannot support the microgrid during this mode. Hence EMS shifted to load shedding mode and charged the battery. The SC will charge if the SC voltage is less than 50% as shown in Fig. 5.

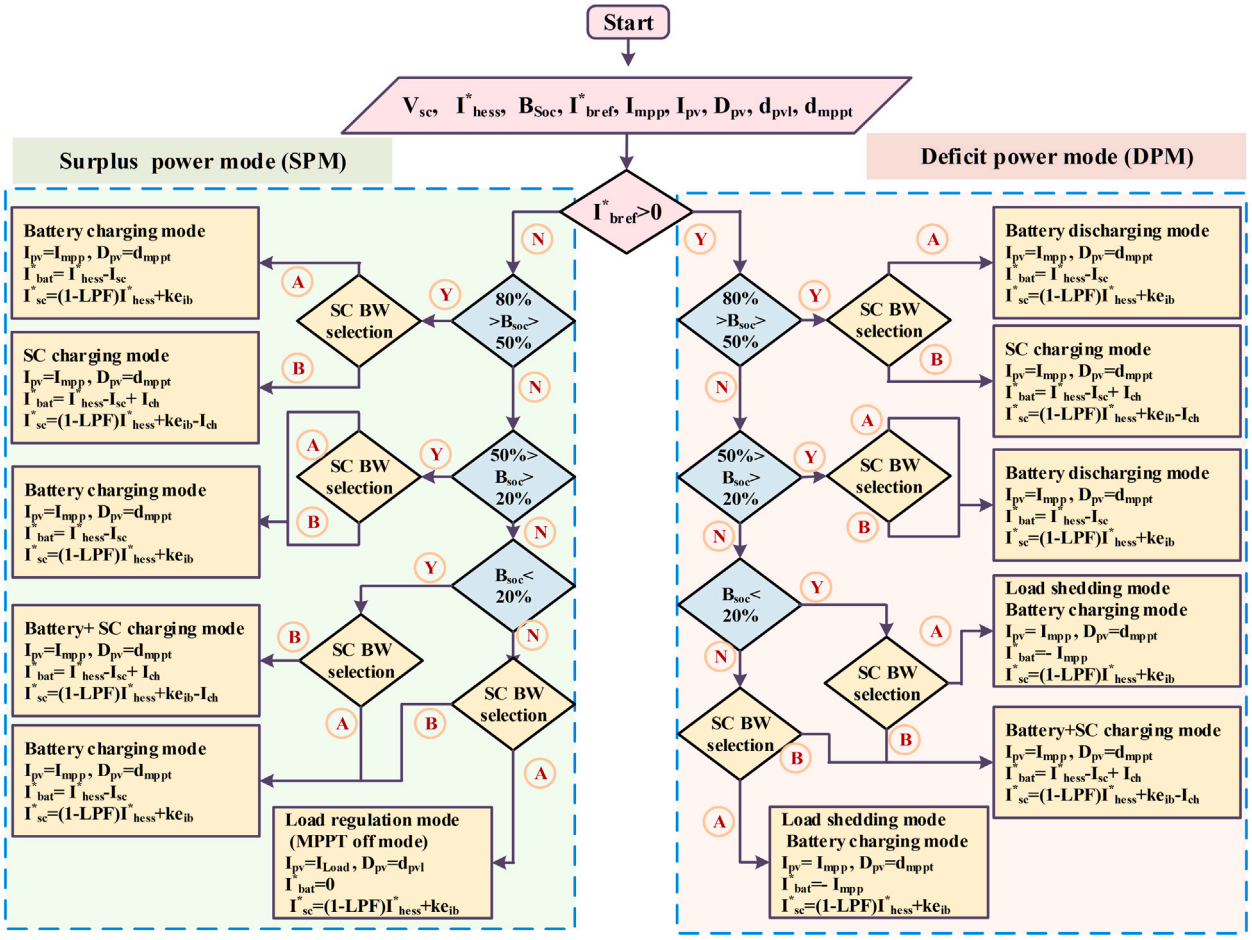

Fig. 5. Block diagram representation of VBLPF based supercapacitor energy management strategy.

Mode-IV $B_{soc} > 80\%$: In this mode, the battery is overcharged. This mode shifts the PV control from MPPT to voltage regulation mode to maintain the load voltage. The SC is allowed to charge from the battery if the SC voltage is less than 50% as depicted in Fig. 5.

(2) Surplus power mode, $(I_{bref} * < 0)$: In SPM, the PV power is greater than load demand. Hence, the average reference current, $I_{bref} *$ is less than zero. There are four sub-modes to describe SPM explained as following. This mode enables the charging of the battery and SC unit.

Mode-IV $50\% < B_{soc} < 80\%$ In this mode, the total PV power is more than load demand. The SC can supply or absorb transients up to 50% of SC voltage and preferred to charge below that range.

Mode-VI $20\% < B_{soc} < 50\%$: If the SC voltage is dropped below 50%, it enables the charging of SC along with battery.

Mode-VII $B_{soc} < 20\%$ If the battery power reduced below limits it need to get charged. This mode sheds the loads and charges the battery. If the SC power is less than 75%, then SC is kept in charging mode.

Mode-VIII $B_{soc} > 80\%$ In this mode, the battery power reached the upper limit. PV will shift to load regulation mode. SC charges from the supply if the SC voltage is less than 50%.

4. Analysis of PV-DC microgrid control strategy

The microgrid control generates the control signals for the PV converter and HESS bidirectional converters. The proposed HESS control strategy is modeled and analyzed using Matlab/Simulink. The PV is regulated by MPPT and HESS is controlled based on proposed EMS. The HESS controllers parameters are derived using uncompensated loop transfer functions given in Table 1 [32].

4.1. PV control strategy

The primary goal of the MPPT algorithm is to obtain maximum power from the PV panel. The most basic and conventional MPPT technique is the perturb and observe (P&O) method. In this method, the duty ratio is varied in steps based on output voltage to obtain the maximum power point. The flowchart for the P&O method and P-V curve is depicted in Fig. 6(a) and (b). At normal operation, the P&O technique generates the required duty signal (d_{pv1}) for extracting maximum power. Excess power mode with 80% battery SOC (Mode-IV) causes the PV to switch to load regulation mode. The PV boost converter control signals (d_{pv2}) are generated using PI_{pv}. Where PI_{pv} is the PV voltage controller and is given by,

$$PI_{pv} = K_{ppv} + \frac{K_{ipv}}{s} \tag{1}$$

The K_{ppv} and K_{ipv} values are 0.35 and 20 respectively. The proposed EMS select the required duty pulse based on available energy and SC voltage.

4.2. HESS reference current generation

In the HESS controller, the reference current generation needs to ensure that the power supplied by HESS and PV must meet the load demand. The power generated by the PV source is independent of the load demand during MPPT mode. Hence the HESS has to supply the deficit power during a reduction in PV generation and store the surplus power during excess PV generation. The relation between HESS and load current can be addressed as follows:

$$i^*_{hess} = i^*_{bat} + i^*_{sc} = i^*_{tot} - i_{pv} \tag{2}$$

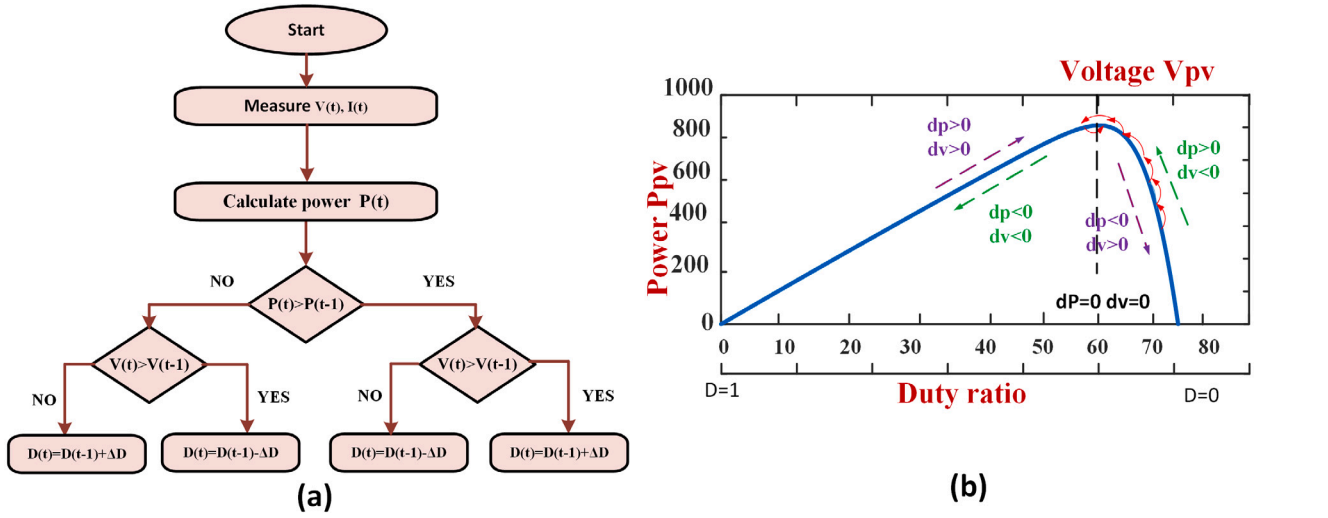

Fig. 6. PV control strategy: (a) P&O MPPT algorithm flow chart (b) P–V characteristics with duty.

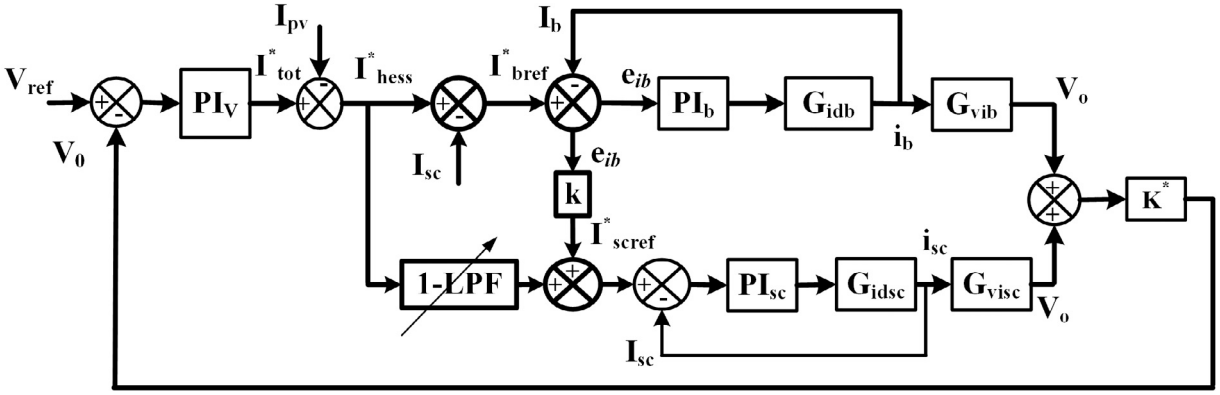

Fig. 7. Small signal block diagram of proposed HESS control scheme.

Where, $i^*_{HESS} = i_{bat} + i_{sc} = i_{tot} - i_{pv}$ are the total HESS current reference, battery current reference, SC current reference, total current reference and PV current generated. The battery and SC reference currents are generated based on the proposed power splitting scheme. The average component of HESS reference current is calculated by:

$$i^*_{bat} = i^*_{hess} - i_{sc} \tag{3}$$

$$i^*_{sc} = i^*_{hess}(1 - LPF) + ke_{ib} \tag{4}$$

where i_{sc}, i_{bat}, V_b, V_{sc} and e_{ib} are the actual SC current, battery voltage, SC voltage and battery current error. The gain k is used to limit the current error, and it is given as $\frac{V_b}{V_{sc}}$. The actual SC current is used to calculate the battery reference current. The SC reference current is the sum of uncompensated battery current and the transient part of the total HESS reference current. According to Eq. (4), the SC current generation varies with SC voltage and VBLPF BW.

4.3. Battery current controller

The battery current controller forces the battery current to follow the slow-changing reference current. The controller is designed based on the duty to control transfer function (G_{idb}) of the battery, which is given in Table 1. The block diagram for control system modeling is shown in Fig. 7. The battery inductor current is calculated from error as written below:

$$i_b = e_{ib} PI_b G_{idb} \tag{5}$$

Where PI_b is the battery current controller and is given by,

$$PI_{ib} = K_{pib} + \frac{K_{iib}}{s} \tag{6}$$

The e_{ib} is the battery current error and is given by,

$$e_{ib} = i^*_b - i_b \tag{7}$$

K_{pib} and K_{iib} are the battery current PI controller gains. The battery current loop is made faster than the voltage control loop and slower than the SC current loop by adjusting the bandwidth. It helps to slow down the battery current during the disturbances. The bandwidth and phase margin of the battery current loop is selected as 10 k rad/sec and 60°, respectively. The bode diagram of compensated system in Fig. 8 (a) shows that the controller provides high gain at low frequencies. The low value of integral gain indicates the lower dynamics of the battery current loop.

4.4. SC current controller

The SC current control loop is the fastest in the overall HESS control system. It can deliver/absorb rapid transient power that exists in the DC load bus. The controller design considers the duty to the current transfer function of SC, which is given in Table 1. From the controller block diagram, the SC current calculation is given as:

$$i_{sc} = e_{isc} PI_{sc} G_{idsc} \tag{8}$$

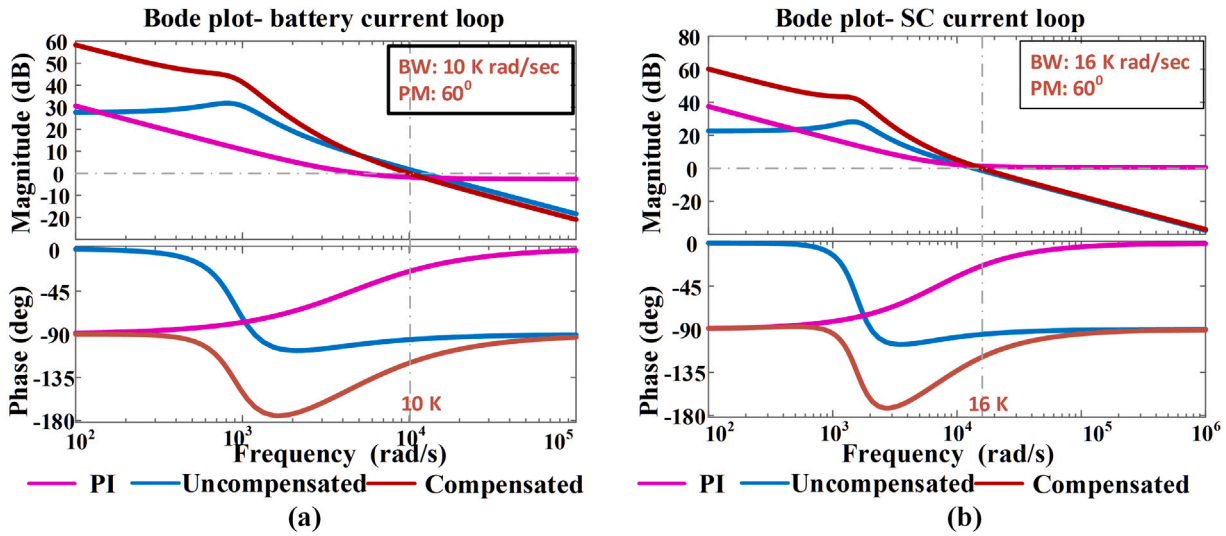

Fig. 8. Bode diagram of uncompensated and compensated system (a) Battery current control loop (b) SC current control loop.

Table 1
System transfer function and controller parameters.

S.No	Control loop	Transfer function	K_p	K_i	B.W (rad/s)	P.M.
1	Battery current loop	$G_{idb} = \frac{\hat{i}_b(s)}{\hat{d}_b(s)} = \frac{C_{0b}V_0 s + 2(1-D_b)I_b}{L_b C_{0b} s^2 + \frac{L_b}{R_L} s + (1-D_b)^2}$	0.65	220	10000	60°
2	SC current loop	$G_{idb} = \frac{\hat{i}_b(s)}{\hat{d}_b(s)} = \frac{C_{0b}V_0 s + 2(1-D_b)I_{bx}}{L_b C_{0b} s^2 + \frac{L_b}{R_L} s + (1-D_b)^2}$	0.833	3733	16000	60°
3	Current to voltage	$G_{vi} = \frac{\hat{V}_0(s)}{\hat{i}_x(s)} = \frac{(1-D)V_0 - LI_x s}{CV_0 s + 2(1-D)I_x}$	0.26	135	600	60°

Table 2
Rating of DC microgrid components.

S.No	Component	Specifications
1	PV panel ratings considered	V_{pv} = 60 V, I_{pv} = 14.7 A
2	SC unit	V_{sc} = 48 V, C_{sc} = 19.3 F
3	DC–DC converter system	L_{pv} = 3.1 mH, L_b = 2.3 mH, L_{sc} = 2.3 mH, C_{0dc} = 430 μF , R_L = 24 Ω
4	Rated output power, P_{out}	1 kW
5	Switching Frequency, f_{sw}	20 kHz
6	Load Voltage, V_0	96 V

Where, e_{isc} is the error in super capacitor current. The SC current controller is represented as PI_{isc} and is written as follows:

$$PI_{isc} = K_{pisc} + \frac{K_{iisc}}{s} \tag{9}$$

The faster dynamics of the SC current loop are achieved by the rigorous design of the current controller. The bandwidth is chosen higher than that of the battery current loop and lower than the switching frequency to avoid the unwanted ripple in the output. As a result, the controller bandwidth is 16 krad/sec, and a phase margin of 60° is selected. From the bode plot shown in Fig. 8 (b), it is clear that the new compensated system is having high gain at low frequencies and low gain at switching frequencies. Thus, it helps to improve the response at the initial period and reduces the ripple amplitude at switching frequency.

4.5. DC bus voltage controller

The outer voltage control loop plays a crucial role in the DC bus regulation. In addition to the delay imposed by LPF, the right-hand zero of the boost converter directly affects the load voltage. Hence the controller parameter selection requires utmost care in the case of the outer loop controller. The outer loop voltage controller is given as:

$$PI_v = K_{pv} + \frac{K_{iv}}{s} \tag{10}$$

The outer voltage controller receives the error between the reference voltage and the actual voltage. To compensate for the corresponding error, the controller generates the total current reference. The outer voltage controller design utilizes the overall transfer function of the system. The outer loop is designed based on the SC control transfer function to reduce complexity in previous works. However, those approaches failed to incorporate battery performance. The combined system model of the proposed control strategy is given as:

$$G_{v,all} = (PI_v G_{vib} + PI_v k G_{visc} + PI_v(1 - LPF)G_{visc})K^* \tag{11}$$

Where: $G_{v,all}$: Overall loop gain of compensated control system
G_{visc}: current to voltage transfer function of SC
G_{vib}: current to voltage transfer function of SC
The‘ gain ‘K^*’ is used to obtain the actual output voltage for the model shown in Fig. 7. The inner current loops are faster than the outer voltage loop and its loop gain is taken as unity. The BW of the outer voltage control loop has the lowest value compared to other control loops so that it decouples the slow variation of capacitor voltage from the fast inner current loops. The phase margin and bandwidth of the control loop are 60° and 600 rad/sec, respectively. The bode diagram for the outer compensated and uncompensated system with variation in VBLPF BW is shown in Fig. 9. From the diagram, an increase in VBLPF BW reduces the system BW and increases the phase margin. At BW= BW6, the control system BW is 453 rad/sec and the phase margin is 71°, ensuring system stability in all VBLPF BW conditions. The controller parameters are designed using MATLAB/SISO tool. The different control loop, transfer functions, controller parameters, bandwidth and phase margin of each control loop are summarized in Table 1.

5. Simulation study

Extensive simulation studies are performed in Matlab/Simulink to validate the performance of HESS with the VBLPF control strategy. The simulation parameters of the microgrid system are shown in Table 2. The proposed control and EMS performance are validated under basic operating scenarios such as (i) sudden change PV irradiation and (ii) sudden change in connected load. The Fig. 10 depict the simulation results of various parameters such as V_0, I_l, I_{pv}, I_b and I_{sc}.

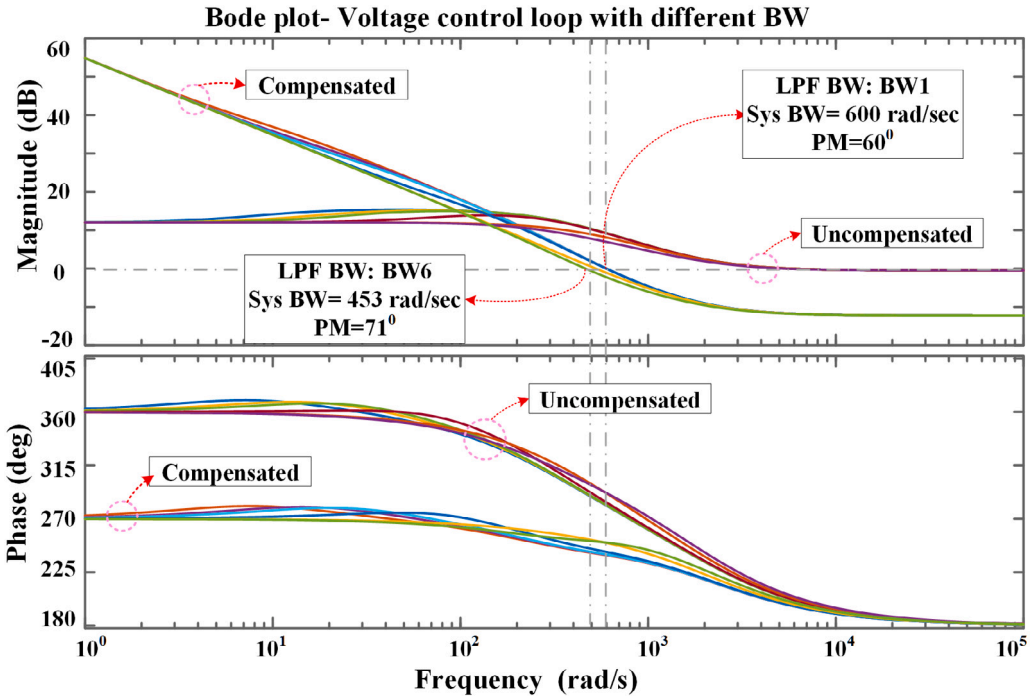

Fig. 9. Bode diagram of uncompensated and compensated system for outer voltage control loop with different BW.

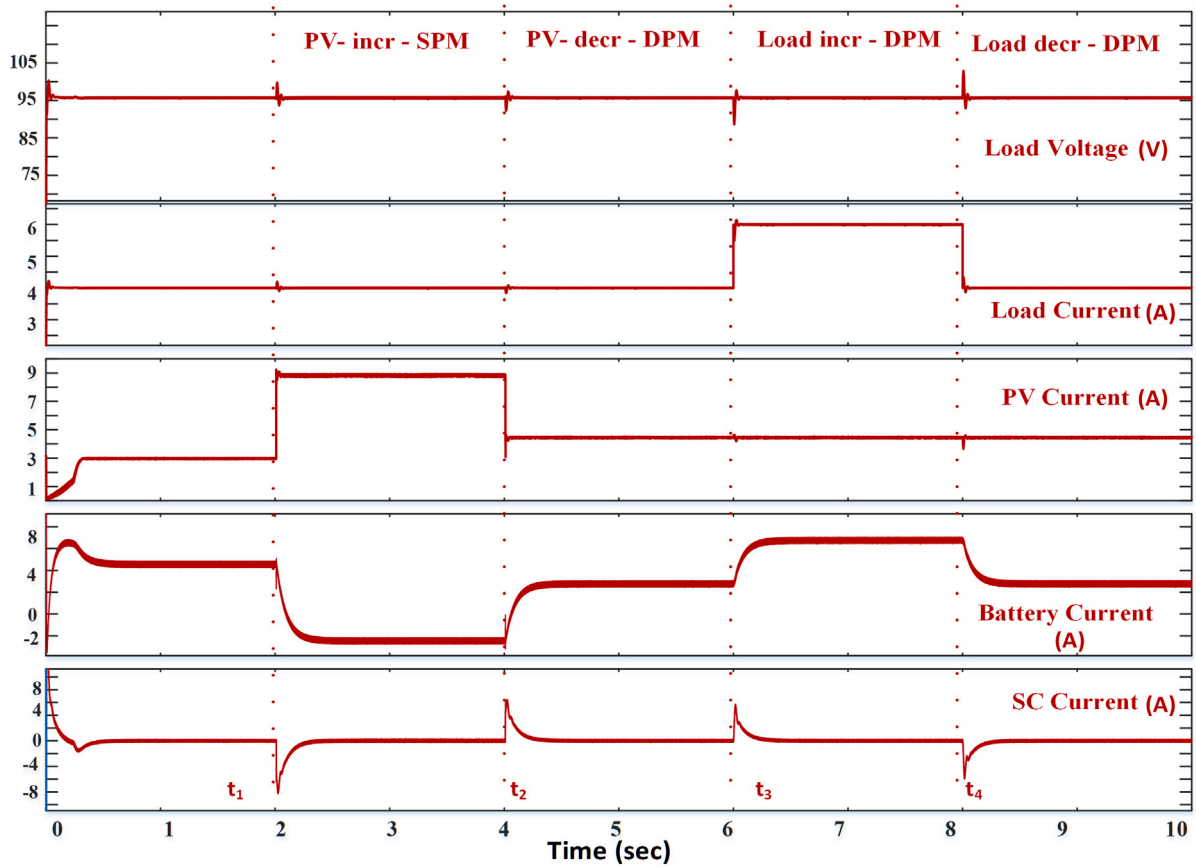

Fig. 10. Simulation results: System performance during sudden change in source and load: $t_1 - t_2$= PV power increased under SPM, t_2= PV power decreased under DPM, t_3= Load increment under DPM, t_4= Load decrement under DPM.

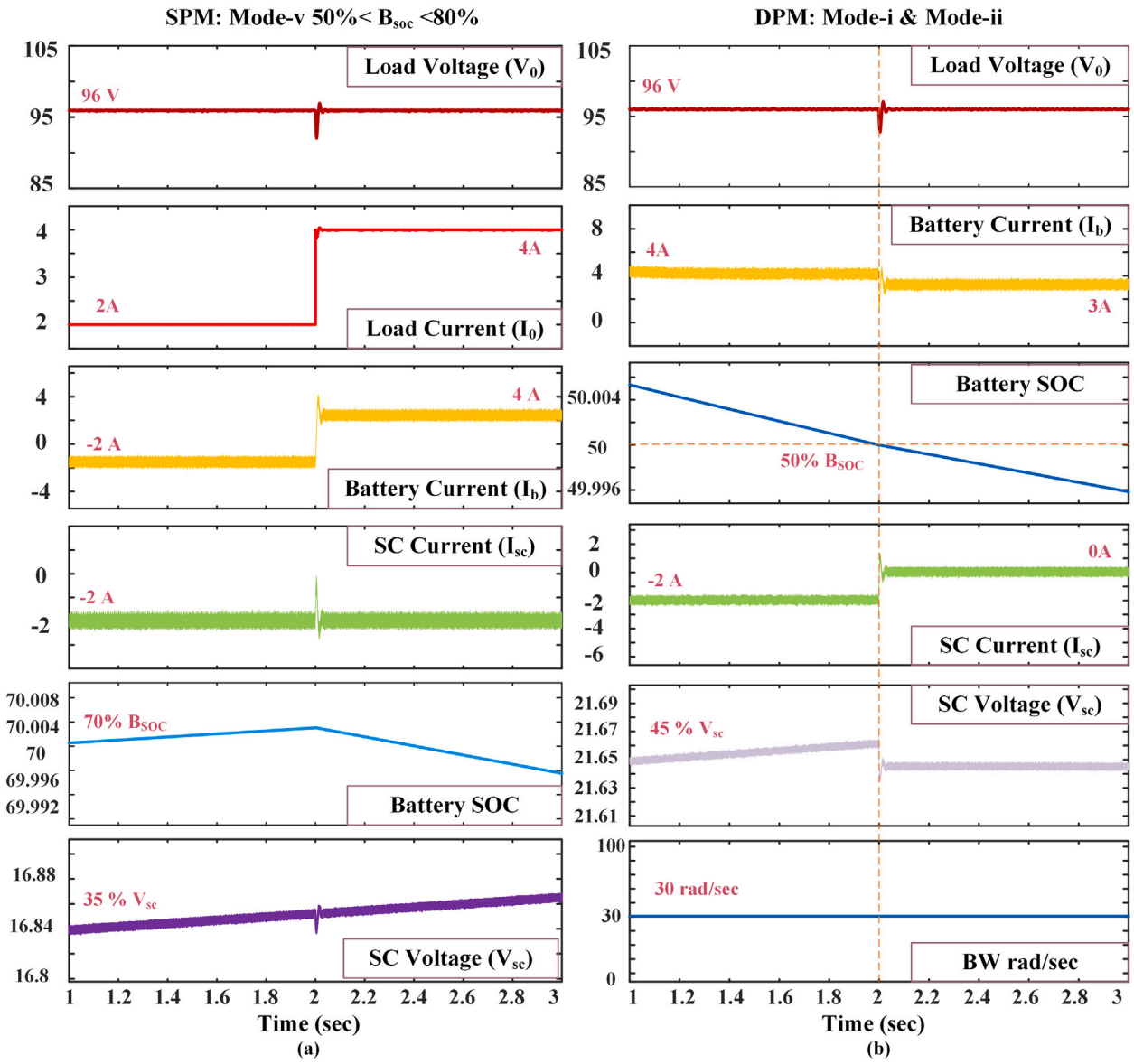

Fig. 11. Simulation study: Performance analysis of EMS at different mode: (a) Mode-I & mode-V (b) Mode-I & Mode-II.

5.1. Performance under the change in PV generation

The system response under step change in PV power generation is applied at t_1 and t_2 as shown in Fig. 10. Initially, the battery and PV together supply the load demand. At t_1, the PV generation is more than load demand (SPM). The surplus power that exists in the DC bus is used to charge the battery. At t_2 instant, the PV generation is reduced to a new lower level with I_{pv}= 4 A. During this period, the battery meets the reduction in load power demand as PV output decreases. It is clear from the waveforms that the DC bus is regulated within the voltage range and that the SC compensates for the rapid power surge generated in the system.

5.2. Performance under the change in load demand

The system response under load change is validated by applying step increment in load demand at t_3 and step decrement at t_4. From Fig. 10, it is clear that load voltage regulates at 96 V in all conditions. The system operates under DPM due to an increase in load demand beyond PV generation. The power difference between load demand and PV generation is used to charge the battery and SC. The SC is fast enough to absorb excess power as the rapid change in battery current is very small. At t_4, the additional load is separated from the DC bus. The power reduction is shared between battery and SC according to the control strategy.

5.3. Operation under different DC microgrid operating modes

The system operates under different modes is tested in simulation. The Mode-V, Mode-I and Mode-II are illustrated in Fig. 11 to analyze the SC charging and mode shifting in the proposed DC microgrid system. Fig. 11(a) shows the mode-v operation under load disturbance. Initially, the SC and battery are charging from PV (Mode-V). At t = 2 s, the load demand increases from 2 A to 4 A. As a result, the battery shift from charging mode to discharging mode and SC remains in charging (Mode-I) due to the availability of battery power. The corresponding B_{soc}, I_{sc}, V_{sc} are depicted in Fig. 11(a). In deficit power mode, if the B_{soc} went below 50%, the SC charging stops due to the reduction in available energy. The corresponding battery current, SC current, Battery SOC, SC voltage and BW are shown in Fig. 11(b). In each mode, the battery and SC operating states are wisely selected based on the EMS. It allows the system to operate for a prolonged duration.

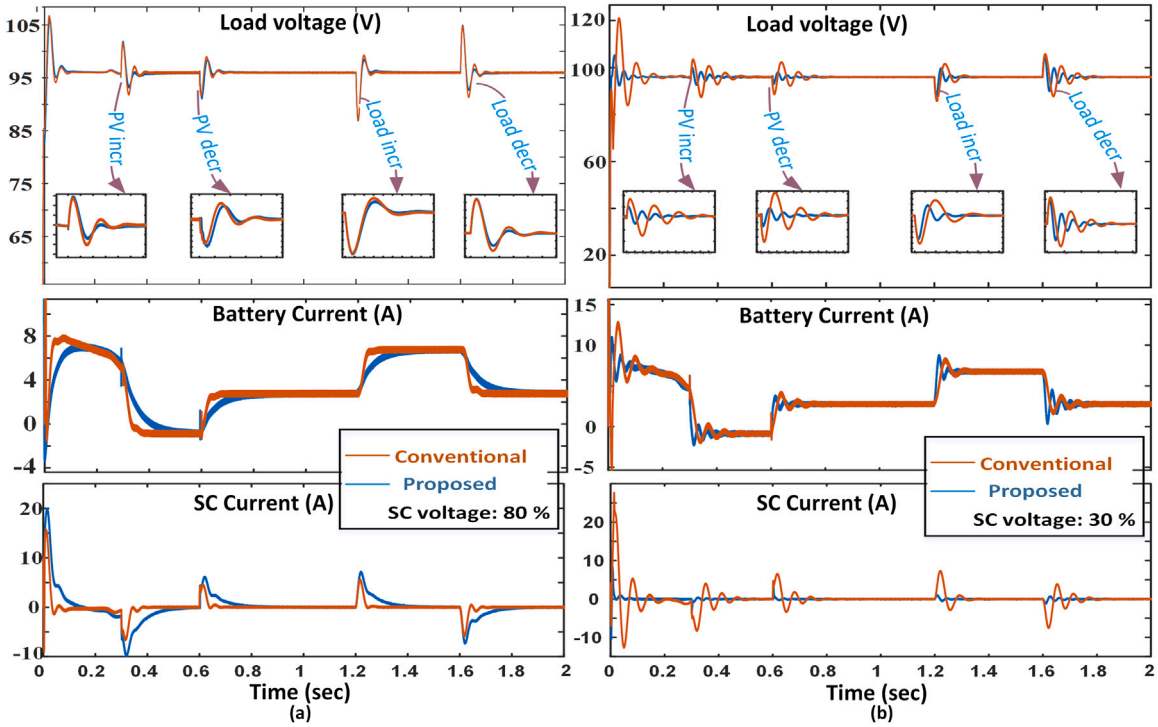

Fig. 12. Simulation study: Comparison of conventional and proposed control strategy with different SC voltages (a) Load voltage, battery current, and SC current at 80% of V_{sc} (b) Load voltage, battery current, and SC current at 30% of V_{sc}.

5.4. Performance comparison of the system under different SC operating voltages

Simulation studies are carried out to compare the performance analysis of HESS control with CBLPF and VBLPF. The conventional and proposed strategies are verified under different DC microgrid conditions. The performance of the system under 80% of SC voltage and 30% of SC voltage are shown in Fig. 12. According to the literature, the bandwidth of the traditional approach is set to 5 Hz [17]. The system performance with fully charged SC shows a similar settling time and peak overshoot as depicted in Fig. 12(a). However, the operation with low SC voltage shows an increase in settling time and peak overshoot at load voltage as shown in Fig. 12(b). The conventional method with 30% SC voltage exhibits the DC bus voltage oscillations for 0.1 s to 0.2 s The maximum peak-to-peak variations for the conventional method are observed at initial transient with 35 V, and the peak is varied between 9 V to 15 V during other system disturbances. On the other hand, the system's operation with VBLPF shows reduced oscillations and faster settling time. The maximum peak-to-peak variation is observed at initial transient with 10 V. All other disturbances create variations less than 10 V. Also, the settling time for DC bus voltage is significantly reduced compared to the conventional method. In the proposed method, the settling time is less than 100 msec for all cases.

The operation of the control strategy is analyzed with similar power splitting strategies presented in Fig. 3. The systems are simulated for the same power level and applied the same disturbances for unity. The obtained results are summarized in Table 3. The traditional PI approach shows overshoot of more than 6% and a settling time between 80% to 120%. The battery error compensation allows the system to reduce the maximum settling time by a factor of 50%. The overall reduction in peak is 3.6% in [18] compared to the conventional method. The proposed method shows much reduction in peak overshoot. The maximum settling time shows a reduction of 66.6% compared to the conventional method. It is relevant to note that the oscillations and peak increases in CBLPF methods as SC voltage increases. The use of VBLPF significantly reduces this effect. Compared to other similar topologies, the proposed method analyzes the variation of SC voltage in the DC microgrid for all scenarios and uses a VBLPF to mitigate the effect.

Table 3
Comparison between proposed controller and traditional PI control methods.

S.No	References	[15]	[18]	[21]	Proposed
1	Maximum peak overshoot (Mp)	6–8.5%	3.8–5.5%	3%–5%	2.6%–5%
2	Settling time (t_{ss}) (ms)	80–120	30–60	30–50	25-40
3	Power splitting strategy	CBLPF	CBLPF	CBLPF	VBLPF
4	Control strategy	PI	PI	PI	PI
5	EMS	YES	NO	YES	YES
6	Consideration of V_{sc} variation	NO	NO	NO	YES

In summary, the simulation results show faster settling and power sharing at different variations applied in the system. The operation under different SC voltages and modes shows that the system regains its stability after disturbance. Further, the charging of SC has a more negligible effect on DC bus voltage variations and SC can absorb transients during this period. The operation with lower SC voltages shows fewer oscillations for the proposed method compared to the conventional method. The proposed EMS allows the stable operation of the DC microgrid system without disconnecting the SC units during lower SC voltage ranges.

6. Experiment results and discussion

Fig. 13 illustrates the experimental setup of PV-DC microgrid integrated with HESS. It comprises a controlled DC power supply with rating 30 V, 5 A for PV module, battery unit consisting of 12 V, 7 Ah lead–acid battery, and Maxwell SC unit with rating 16 V, 58 F. The converters have a 200 W capacity. Due to source limitation

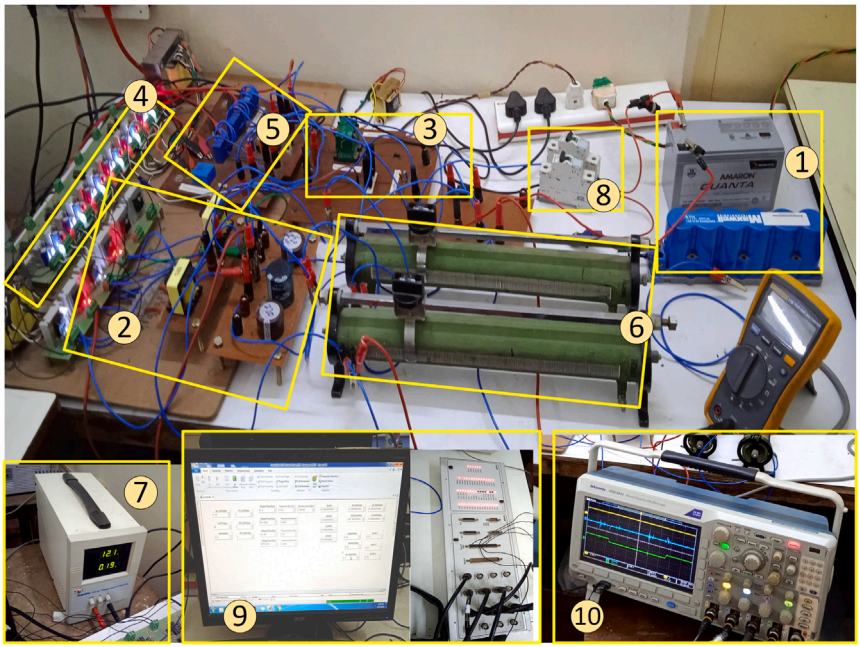

Fig. 13. Experimental prototype developed for the proposed system.

and inductor saturation above 5 A, the nominal operating power is selected as 48 W. The proposed control algorithm and SC energy management are implemented in the dSPACE 1104 control platform. The test system's performance is analyzed with (i) increment in PV generation (ii) decrement in PV generation (iii) increment in load variation and (iv) decrement in load variation. Further, the SC-based EMS is verified experimentally under different SC voltage ranges. The experimental results for wide SC voltage ranges and different power levels are presented to validate the proposed strategy.

6.1. Operation with proposed EMS with 50%–75% charged SC unit

In this mode, the SC voltage is less than 75%. Hence the cut-off frequency of VBLPF is automatically selected as 20 rad/sec. During this period, the SC unit provides almost zero current at steady-state and responds instantaneously to the disturbances. Hence the change in SC voltage is minimal as the PV and battery supply the total load power demand. However, the sudden changes in PV generation or load demand create a power imbalance in the DC bus. The fast action of controllers controls the flow of deficit or surplus power in the DC bus and EMS regulates the power balance in the system. The following section analyzes the DC microgrid with 50%–75% charged SC unit operation under different interruptions.

6.1.1. Change in PV generation

The experiment is carried out for three different PV generation circumstances as shown in Fig. 14(a). Firstly PV generation is made more than load demand. As a result, the excess power in the DC bus charges the battery during the t_0 to t_1 period. The load demand is 1 A and PV current is 3 A. The battery current is negative during the period indicating that the battery is charging from a PV source. At t_1, the PV generation is changed to 1 A. The battery current is increased to 1 A to meet the load demand. It is important to infer from the waveform that the SC supplies the initial current to allow the slow change in battery current. At $t = t_3$, the PV generation increases to 2 A and meets the load requirement. As a result, the battery current gradually decreases to zero, while the SC absorbs the excess current supplied by the battery. Hence, the SC limits the sudden variation in battery current and reduces the stress on battery. In all cases, the EMS balance the power between PV, battery, SC and load, and the DC bus oscillations are mitigated.

6.1.2. Change in load demand

Fig. 14(b) illustrates the operation of DC microgrid under varying load conditions. Compared to PV variations, the load variations introduce more oscillations on DC bus voltage. A 100% change in load is applied to verify the proposed scheme. The power supplied by PV panel is 12 W, (V_{pv}= 12 V and I_{pv}= 1 A). The required load power at t_0 is 24 W and the battery supplies the remaining 12 W power. This is illustrated in the time period t_0 to t_1. At t_1, the load demand increased to 2 A. To fulfill the load demand, the battery current increases to 3 A. Since the change in battery current is limited, the SC supplies the transient current. At t_2, the load demand reduces to 1 A. The results show that the proposed EMS ensures DC voltage regulation and the power balance achieved between load, PV, battery, and SC based on available power.

The proposed strategy is analyzed under different loading conditions. The operation with 7 W and 15 W load demand is shown in Fig. 14(c). The battery is initially in charging mode and changed to discharging mode after load disturbance. The variation in supercapacitor voltage and current analysis is depicted in Fig. 14(d). The SC voltage is 12 V and the supercapacitor absorbs the transient current of 0.5 A at the time of disturbances. The battery current changes from 1 A to 0.5 A at the time of load reduction. The operation and current sharing during 6 W to 12 W power variations is shown in Fig. 15(a). Further, the PV voltage is maintained at 12 V during operation and battery absorbs the excess power generated during increment in PV generation as shown in Fig. 15(b). The DC microgrid operation with measured battery voltage is shown in Fig. 15(c). In the above two cases, the battery and SC voltage is maintained constant irrespective of the disturbances in the system.

A summary of DC microgrid operation under different PV generation and load demand is presented in Fig. 15(d). At t_1 and t_2, the load demand is varied by 0.5 A. At t_3 and t_4, the PV generation is varied by 1 A. All the excess and deficit power demands are balanced by battery. The sc compensates for the transient power demand. It is significant to note that the DC bus voltage is kept constant at 24 V, regardless of the change in load and source disturbances.

6.2. Operation of proposed EMS with 25–37.5% SC voltage

The proposed control algorithm and SC EMS are verified with lower SC voltage ranges. The cutoff frequency of VBLPF is 100 rad/sec. A

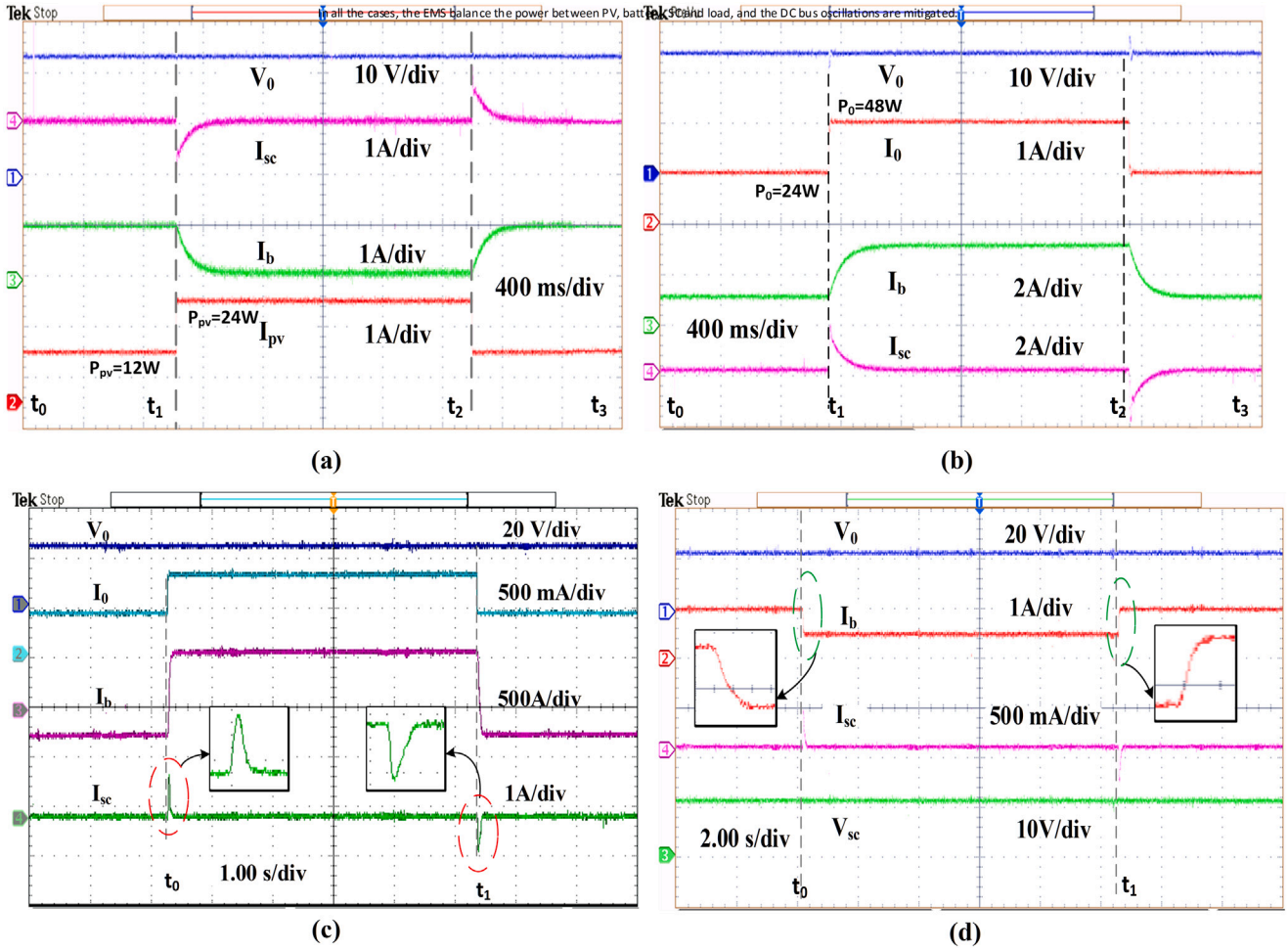

Fig. 14. Experimental results with 50%–75% SC voltage: (a) system under PV disturbance:load voltage, battery current, SC current, PV current (b) system under load disturbance:load voltage, load current, battery current, SC current (c) Load power variation from 12 W to 24 W (d) SC voltage and SC current during disturbances.

100% load disturbance is applied to verify the system performance with lower SC voltage and VBLPF as shown in Fig. 16(a). The SC is supplying the transient current of 300 mA and the battery is supplying a steady-state current of 2 A. PV current increment and decrement of 0.8 A is applied to the DC microgrid system as shown in Fig. 16(b). The battery changed from discharging to charging state and SC supplies the transient current with a maximum amplitude of 400 mA. The DC bus voltage is maintained at 24 V irrespective of the variations in load demand and SC voltage.

The system performance is compared with conventional CBLPF control and proposed VBLPF control as shown in Fig. 16(c) and (d). The SC operating voltage is 4.8 V and the battery voltage is 12 .2 V. The load demand is increased by 0.5 A and the battery discharges 1 A to meet the load demand. During disturbances, there is an increase in the settling time, and the ringing effect occurs at DC bus voltage due to the application of a CBLPF with lower SC voltage. The increase in the settling time and the ringing effect reduces with the help of VBLPF such that the DC bus voltage settled faster and maintained constant throughout the period. Compared to the conventional method, the proposed method has fewer oscillations in the battery current, supercapacitor current, and DC bus voltage as shown in Fig. 16(d).

6.3. Operation with SC charging condition

The charging operation of SC in proposed microgrid conditions is discussed in this section. The SC voltage regulation plays an important role in the HESS energy management strategy. The SC voltage has to charge and discharge based on a particular range of voltage levels. The proposed system operation is depicted in Fig. 17(a). The SC voltage is 4.2 V and the battery is in charging mode during operation. The SC absorbs/delivers less energy since the SC voltage is less than 50%. The DC bus voltage has little spikes during disturbances and settles as fast as possible. The charging is depicted in Fig. 17(b). At t = t_1, SC charging is enabled, the SC voltage is seen to be rising and the SC inductor current is seen to be flowing in the negative direction, indicating the charging of SC. At t_2, the load disturbance is applied with battery current demand of 1 A. The load demand is removed at t_2. It is clear from the waveforms that the SC charging is unaffected during disturbances. Further, the battery current is changing smoothly and DC bus voltage has fewer oscillations during operation. The SC voltage is rising from 4.8 V and reached 5.1 V during this period.

A summary of hardware studies at different operating points is summarized in Table 4. The analysis presents total power demand and measured voltage and current through the PV, battery, SC and DC loads. With the proposed control method, the effect of variation in SC voltage is limited by regulating the SC reference current using VBLPF. The operation with 73% SC voltage provides more transient current during disturbance. The SC charging current is 0.5 A and transient current during charging is around 0.25 A.

In brief, the experimental results agree with the simulation study. The battery and SC share the excess/deficit power that exists in the DC bus. The battery supplies or absorb the average power and SC compensates for the transient power. Hence SC reduces the sudden current stress on the battery and improves the battery life. Further,

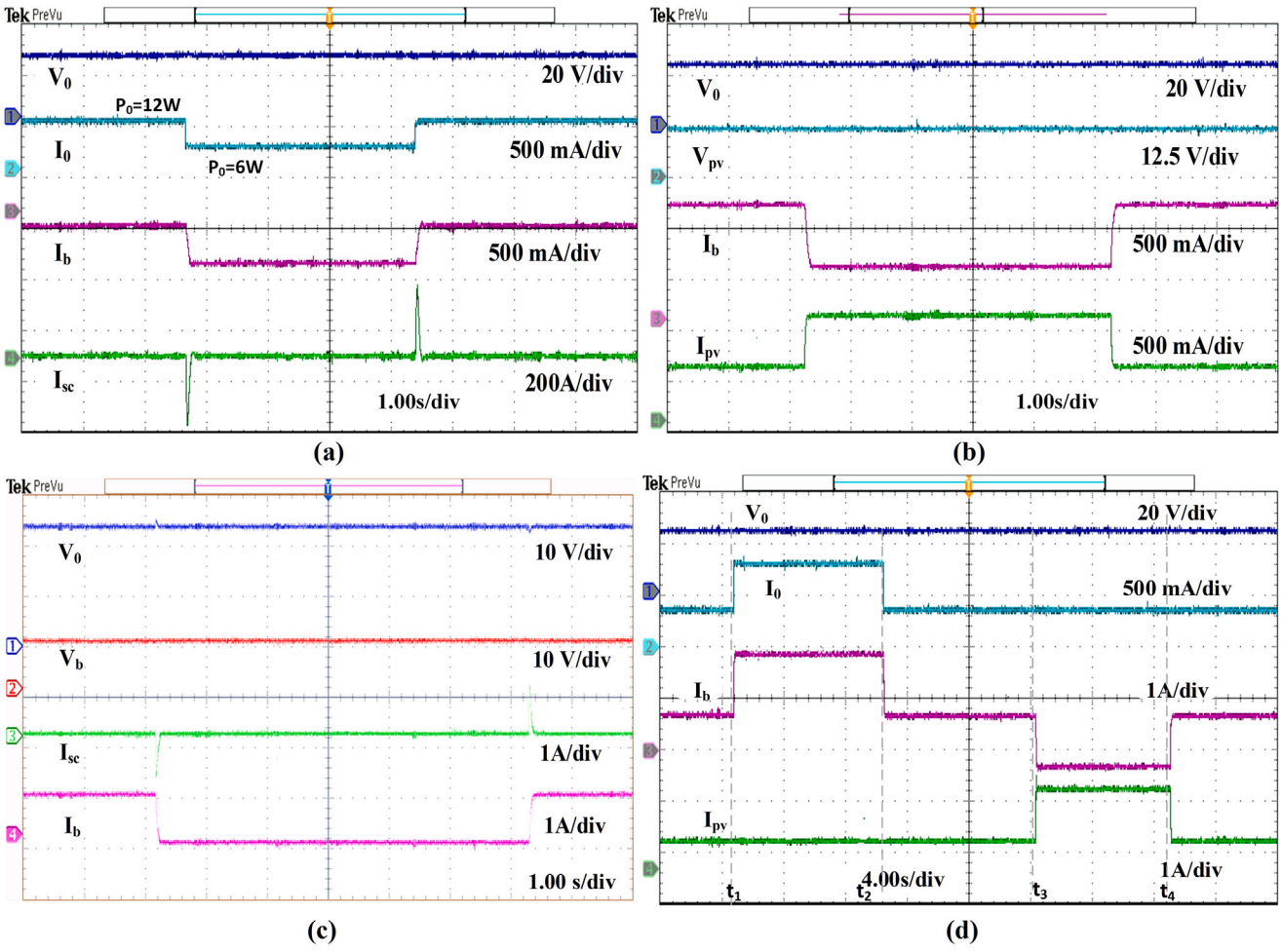

Fig. 15. Experimental results with 50%–75% SC voltage: (a) Experimental results for 6 W to 12 W power variation (b) PV voltage, PV current, load voltage and battery current during PV variation (c) Battery voltage, Battery current, SC current and DC bus voltage during load change (d) system operation under load disturbance and PV disturbance together.

Table 4
A summary of hardware results at different operating points.

Load Power (W)	V_0 (V)	I_0 (A)	V_{pv} (V)	I_{pv} (A)	V_b (V)	I_b (A)	V_{sc} (V)	I_{sc} (Average) (A)	I_{sc} (transient) (A)
48	24	2	12	2	12.2	2	11.8	0	0.8–1
48	24	2	12	2	12.2	2	4.8	0	0.2–0.4
24	24	1	12	1.4	12.2	0.6	11.8	0	0.5–0.7
24	24	1	12	1.4	12.2	0.6	4.8	0	0.2–0.4
12	24	0.5	12	0.5	12.2	0.5	11.8	0	0.3–0.6
12	24	0.5	12	0.5	12.2	0.5	4.8	0	0.1–0.3
6	24	0.25	12	0.3	12.2	0.2	11.8	0	0.2–0.3
6	24	0.25	12	0.3	12.2	0.2	4.8	0	0.1–0.2
SC charging	24	0.5	12	1	12.2	1.4	4.8	−0.5	0.1–0.25

compared to the conventional CBLPF method, the proposed VBLPF method effectively minimizes the effect of SC voltage variation such as ringing in DC bus voltage and oscillations in battery and SC currents. Hence the VBLPF method effectively manages SC voltage variation and reduces the oscillations thereby improving the battery life during lower SC voltages. Further, the mode shifting due to PV power variation, load variation, and SC charging have less effect on DC bus voltage. The proposed charging scheme shows the charging of SC without affecting DC bus voltage even under disturbances. Hence the VBLPF control scheme provides better DC bus voltage regulation and SC voltage handling in DC microgrid operation.

Conclusion

A novel control scheme with an SC energy management strategy is proposed for an isolated PV-DC microgrid with HESS. The proposed control strategy successfully separates the LPF effect from the battery control loop and the VBLPF based EMS leads to better SC utilization at different SC voltage ranges. The developed EMS addresses the DC microgrid in various operating modes and produces a stable and desirable performance. Both the battery and the SC effect on the control loop are considered while modeling the device and designing the outer voltage controller. The HESS is implemented with MPPT controlled PV-DC microgrid and verified for different source and load variations. In contrast to the traditional approach, the simulation and experimental

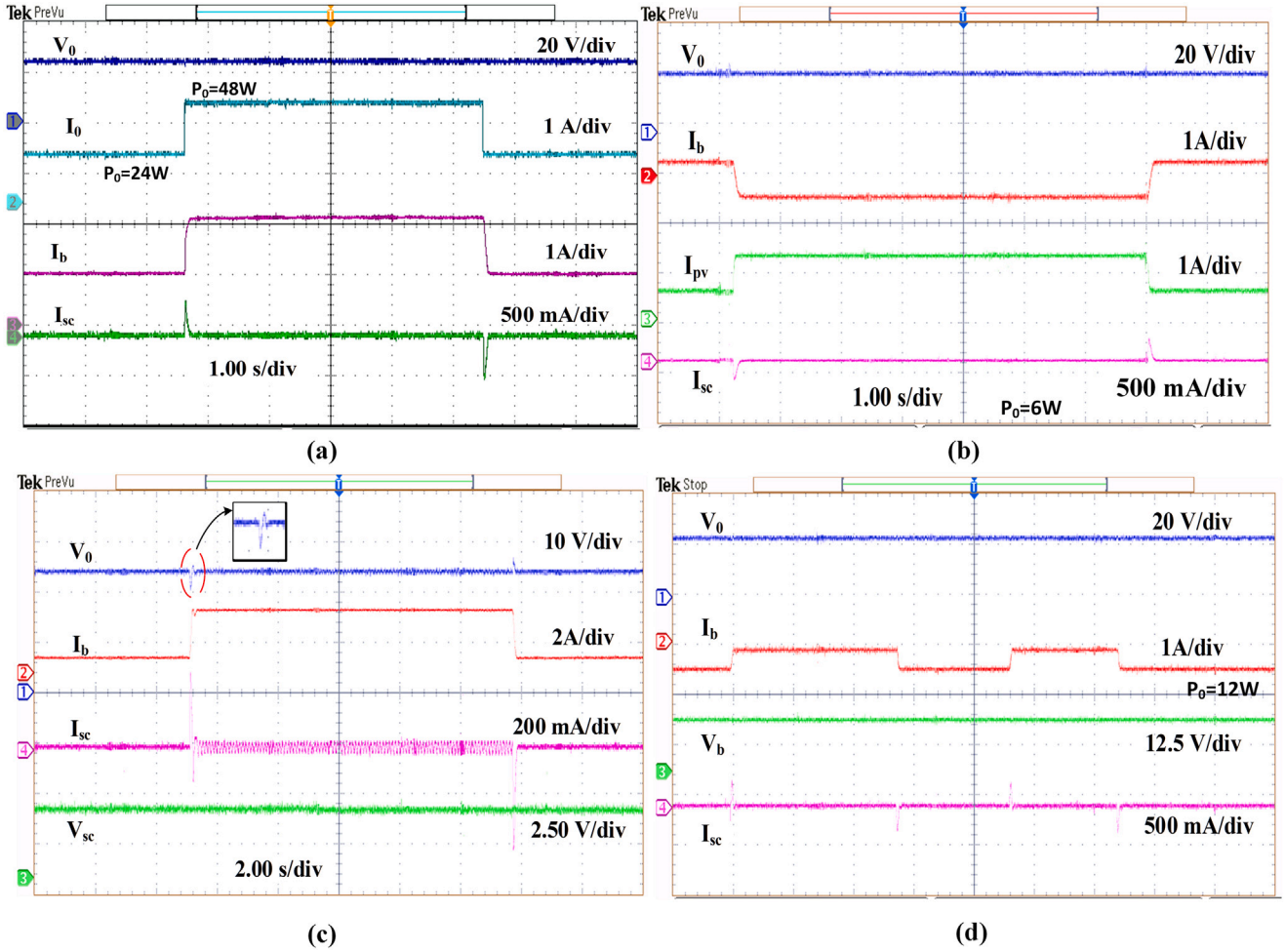

Fig. 16. Experimental results with 30% SC voltage: (a) Load voltage, load current battery current and SC current during load disturbance (b) Load voltage, PV current battery current and SC current during PV disturbance (c) Oscillations in load voltage and SC current in conventional PI-LPF control strategy (d) battery voltage and current during load disturbance.

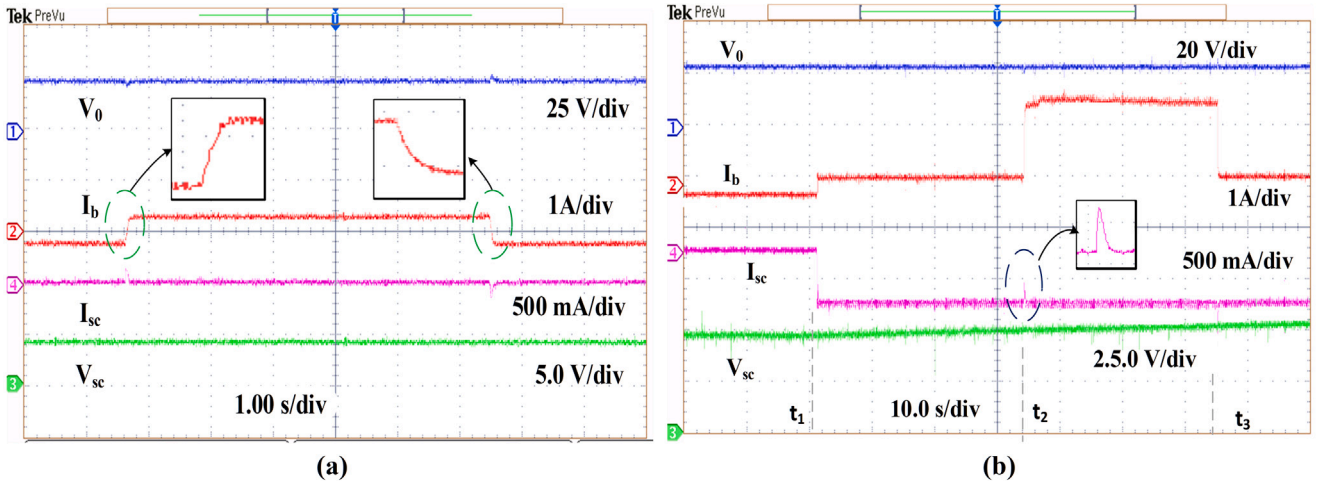

Fig. 17. Experimental results with 30% SC voltage: (a) Load voltage, battery current, SC voltage and SC current under proposed control (b) Charging of SC and DC bus voltage regulation during load disturbance.

results validate the effectiveness of the proposed system in reducing the oscillations at DC bus voltage and improving the transient and steady-state performances. Several features are illustrated, including quick DC bus voltage regulation, reduced battery current stress, SC charging operation, and mode shift. The system parameters are maintained as per limits during operation, disturbances and mode changes. Furthermore, the suggested EMS eliminates the need for weather forecasts and load current/power measurements, reducing the complexity and number of sensors.

Declaration of competing interest

The authors declare that they have no known competing financial interests or personal relationships that could have appeared to influence the work reported in this paper.

References

[1] Z. Shuai, J. Fang, F. Ning, Z.J. Shen, Hierarchical structure and bus voltage control of DC microgrid, Renew. Sustain. Energy Rev. 1 (82) (2018) 3670–3682, http://dx.doi.org/10.1016/j.rser.2017.10.096.

[2] G. Dileep, S.N. Singh, Maximum power point tracking of solar photovoltaic system using modified perturbation and observation method, Renew. Sustain. Energy Rev. 50 (2015) 109–129, http://dx.doi.org/10.1016/j.rser.2015.04.072.

[3] A. Foles, L. Fialho, M. Collares-Pereira, Techno-economic evaluation of the Portuguese PV and energy storage residential applications, Sustain. Energy Technol. Assess. 39 (2020) 100686, http://dx.doi.org/10.1016/j.seta.2020.100686.

[4] Nihal Kularatna, Kosala Gunawardane, 2 - fundamentals of energy storage devices, editor(s): Nihal kularatna, kosala gunawardane, in: Energy Storage Devices for Renewable Energy-Based Systems, Second Ed., Academic Press, ISBN: 9780128207789, 2021, pp. 37–64, http://dx.doi.org/10.1016/B978-0-12-820778-9.00005-X.

[5] A.O. Gbadegesin, Y. Sun, N.I. Nwulu, Techno-economic analysis of storage degradation effect on levelised cost of hybrid energy storage systems, Sustain. Energy Technol. Assess. 36 (2019) 100536, http://dx.doi.org/10.1016/j.seta.2019.100536.

[6] C.R. Arunkumar, U.B. Manthati, Design and small signal modelling of battery-supercapacitor HESS for DC microgrid, in: TENCON 2019-2019 IEEE Region 10 Conference, TENCON, IEEE., 2019, pp. 2216–2221, http://dx.doi.org/10.1109/TENCON.2019.8929544.

[7] D. Alvaro, R. Arranz, J.A. Aguado, Sizing and operation of hybrid energy storage systems to perform ramp-rate control in PV power plants, Int. J. Electr. Power Energy Syst. 107 (2019) 589–596, http://dx.doi.org/10.1016/j.ijepes.2018.12.009.

[8] C.R. Arunkumar, U.B. Manthati, S. Punna, Supercapacitor-based transient power supply for DC microgrid applications, Electr. Eng. 24 (2021) 0–1, http://dx.doi.org/10.1007/s00202-021-01312-7.

[9] U. Akram, M. Nadarajah, R. Shah, F. Milano, A review on rapid responsive energy storage technologies for frequency regulation in modern power systems, Renew. Sustain. Energy Rev. 120 (2020) 109626, http://dx.doi.org/10.1016/j.rser.2019.109626.

[10] Q. Sun, D. Xing, H. Alafnan, X. Pei, M. Zhang, W. Yuan, : DEsign and test of a new two-stage control scheme for SMES-battery hybrid energy storage systems for microgrid applications, Appl. Energy 253 (2019) 113529, http://dx.doi.org/10.1016/j.apenergy.2019.113529.

[11] J. Hou, Z. Song, H.F. Hofmann, J. Sun, Control strategy for battery/flywheel hybrid energy storage in electric shipboard microgrids, IEEE Trans. Ind. Inf. 17 (2) (2020) 1089–1099, http://dx.doi.org/10.1109/TII.2020.2973409.

[12] S. Barcellona, L. Piegari, A. Villa, Passive hybrid energy storage system for electric vehicles at very low temperatures, J. Energy Storage 1 (25) (2019) 100833, http://dx.doi.org/10.1016/j.est.2019.100833.

[13] E.M. Asensio, G.A. Magallán, CH. De Angelo, F.M. Serra, Energy management on battery/ultracapacitor hybrid energy storage system based on adjustable bandwidth filter and sliding-mode control, J. Energy Storage 1 (30) (2020) 101569, http://dx.doi.org/10.1016/j.est.2020.101569.

[14] Z. Song, J. Li, X. Han, L. Xu, L. Lu, M. Ouyang, H. Hofmann, Multi-objective optimization of a semi-active battery/supercapacitor energy storage system for electric vehicles, Appl. Energy 15 (135) (2014) 12–24, http://dx.doi.org/10.1016/j.apenergy.2014.06.087.

[15] C.R. Arunkumar, U.B. Manthati, P. Srinivas, Accurate modelling and analysis of battery–supercapacitor hybrid energy storage system in DC microgrid systems, Energy Syst. (2021) 1–19, http://dx.doi.org/10.1007/s12667-021-00467-3.

[16] Zineb Cabrane, Dania Batool, Jonghoon Kim, Kisoo Yoo, Design and simulation studies of battery-supercapacitor hybrid energy storage system for improved performances of traction system of solar vehicle, J. Energy Storage (ISSN: 2352-152X) 32 (2020) 101943, http://dx.doi.org/10.1016/j.est.2020.101943.

[17] U. Manandhar, N.R. Tummuru, S.K. Kollimalla, A. Ukil, G.H. Beng, K. Chaudhari, Validation of faster joint control strategy for battery-and supercapacitor-based energy storage system, IEEE Trans. Ind. Electron. 65 (4) (2017) 3286–3295, http://dx.doi.org/10.1109/TIE.2017.2750622.

[18] S. Punna, U.B. Manthati, A. Chirayarukil, Modeling, analysis, and design of novel control scheme for two-input bidirectional DC-DC converter for HESS in DC microgrid applications, in: International Transactions on Electrical Energy Systems, e12774, http://dx.doi.org/10.1002/2050-7038.12774.

[19] H. Guentri, T. Allaoui, M. Mekki, M. Denai, Power management and control of a photovoltaic system with hybrid battery-supercapacitor energy storage based on heuristics methods, J. Energy Storage 1 (39) (2021) 102578, http://dx.doi.org/10.1016/j.est.2021.102578.

[20] S.K. Kollimalla, M.K. Mishra, A. Ukil, H.B. Gooi, Dc grid voltage regulation using new HESS control strategy, IEEE Trans. Sustain. Energy 8 (2) (2016) 772–781, http://dx.doi.org/10.1109/TSTE.2016.2619759.

[21] M.C. Joshi, S. Samanta, Improved energy management algorithm with time-share-based ultracapacitor charging/discharging for hybrid energy storage system, IEEE Trans. Ind. Electron. 66 (8) (2018) 6032–6043, http://dx.doi.org/10.1109/TIE.2018.2871799.

[22] P Singh, J.S. Lather, Dynamic current sharing, voltage and SOC regulation for HESS based DC microgrid using CPISMC technique, J. Energy Storage 30 (2020) 101509, http://dx.doi.org/10.1016/j.est.2020.101509.

[23] Q. Zhang, L. Wang, G. Li, Y. Liu, A real-time energy management control strategy for battery and supercapacitor hybrid energy storage systems of pure electric vehicles, J. Energy Storage 31 (2020) 101721, http://dx.doi.org/10.1016/j.est.2020.101721.

[24] Z. Cabrane, M. Ouassaid, M. Maaroufi, Battery and supercapacitor for photovoltaic energy storage: A fuzzy logic management, IET Renew. Power Gener. 11 (8) (2017) 1157–1165, http://dx.doi.org/10.1049/iet-rpg.2016.0455.

[25] J. Faria, J. Pombo, M. Calado, S. Mariano, Power management control strategy based on artificial neural networks for standalone PV applications with a hybrid energy storage system, Energies 12 (5) (2019) 902, http://dx.doi.org/10.3390/en12050902.

[26] Shuo Zhang, Rui Xiong, Fengchun Sun, Model predictive control for power management in a plug-in hybrid electric vehicle with a hybrid energy storage system, Appl. Energy (ISSN: 0306-2619) 185 (2) (2017) 1654–1662, doi.org/10.1016/j.apenergy.2015.12.035.

[27] A. Katnapally, U.B. Manthati, A. Chirayarukil Raveendran, S. Punna, A predictive power management scheme for hybrid energy storage system in electric vehicle, Int. J. Circu. Theory Appl. (2021) http://dx.doi.org/10.1002/cta.3119.

[28] N.R. Tummuru, M.K. Mishra, S. Srinivas, Dynamic energy management of renewable grid integrated hybrid energy storage system, IEEE Trans. Ind. Electron. 62 (12) (2015) 7728–7737, http://dx.doi.org/10.1109/TIE.2015.2455063, 10.

[29] S. Kotra, M.K. Mishra, A supervisory power management system for a hybrid microgrid with HESS, IEEE Trans. Ind. Electron. 64 (5) (2017) 9–3640, http://dx.doi.org/10.1109/TIE.2017.2652345, 16.

[30] S. Kotra, M.K. Mishra, Design and stability analysis of DC microgrid with hybrid energy storage system, IEEE Trans. Sustain. Energy 10 (3) (2019) 1603–1612, http://dx.doi.org/10.1109/TSTE.2019.2891255, 7.

[31] https://www.mathworks.com/help/control/ref/varyinglowpassfilter.html (Accessed 09 December 2020).

[32] R.W. Erickson, D. Maksimovic, Fundamentals of Power Electronics, Springer Science & Business Media, 2017.